

Dear editor and reviewers,

On behalf of my co-authors, we thank you for giving us a chance to revise and improve the quality of our article.

We have read your comments carefully and have made revision. We have tried our best to revise our manuscript according to the comments: "Application of Wave-current coupled Sediment Transport Models with Variable Grain Properties for Coastal Morphodynamics: A Case Study of the Changhua River, Hainan (egusphere-2024-2154)".

The main revisions in the new manuscript are:

1. The parameters of the hydrodynamic model have been presented in a table.
2. Initial conditions for the sediment model and the wave model's open boundaries have been included.
3. Section 3.4.1 has been removed.
4. Additional details regarding the hydrodynamic simulation results have been provided in Section 3.3.
5. Chapter 4 has been thoroughly rewritten.
6. Conclusions has been revised.

Here is a point-by-point response to the comments and concerns (Two reviewers with a total of 23 comments.).

Thank you for taking the time to consider our research and we look forward to hearing from you at your earliest convenience.

Sincerely,

Yuxi Wu

China University of Geosciences, Wuhan,

Wuhan 430074, P.R.China

E-mail: [yuxiwu@cug.edu.cn](mailto:yuxiwu@cug.edu.cn)

### Detailed comments part:

**Point 1:** The authors claim to use a three-dimensional model (lines 131-132) while the equations they present are depth-averaged two dimensional in x and y. It is also never mentioned which model the authors use. Is it a well established and validated one? Is it open-source like e.g., Delft3D and TELEMAC? Is it an in-house one? Please provide this information and where and if it has been implemented for similar applications.

Response: Thank you for pointing out the discrepancy in our manuscript regarding the model description. We sincerely apologize for the error in the equations presented and appreciate the opportunity to clarify and correct this. Equations (1) to (4) have been removed.

We have made the necessary corrections in the manuscript to accurately reflect that we are using the FVCOM (Finite Volume Coastal Ocean Model), a well-established and widely used three-dimensional model for simulating coastal and oceanographic processes. FVCOM source code was obtained from the Marine Ecosystem Dynamics Modeling Laboratory (<http://fvcom.smast.umassd.edu/>). The FVCOM model is indeed open-source and has been extensively validated across a variety of marine and estuarine applications.

The revised sentence now reads as follows:

“..., An unstructured grid, finite volume, regional ocean model FVCOM (Chen et al., 2003) was used to simulate the hydrodynamic background and hydrological features. It has been widely used for the study of coastal oceanic and estuarine circulation (Jiang and Xia, 2016; Huang et al., 2008; Lai et al., 2018; Chen et al., 2008).”

Applications:

Jiang, L., Xia, M.: Dynamics of the Chesapeake Bay outflow plume: Realistic plume simulation and its seasonal and interannual variability. *Journal of Geophysical Research: Oceans*, 121(2): 1424-1445. doi: 10.1002/2015JC011191, 2016.

Chen, C., Liu, H., Beardsley, R. C.: An unstructured grid, finite-volume, three-dimensional, primitive equations ocean model: application to coastal ocean and estuaries. *Journal of atmospheric and*

*oceanic technology*, 20(1): 159-186. doi: 10.1175/1520-0426(2003)020<0159:AUGFVT>2.0.CO;2, 2003.

Chen, C., Xue, P., Ding, P., Beardsley, R. C., Xu, Q., Mao, X., Gao, G., Qi, J., Li, C., Lin, H., Cowles, G., Shi, M.: Physical mechanisms for the offshore detachment of the Changjiang Diluted Water in the East China Sea. *Journal of Geophysical Research: Oceans*, 113(C2). doi: 10.1029/2006JC003994, 2008.

Huang, H., Chen, C., Blanton, J. O., Andrade, F. A.: A numerical study of tidal asymmetry in Okatee Creek, South Carolina. *Estuarine, Coastal and Shelf Science*, 78(1): 190-202. doi: 10.1016/j.ecss.2007.11.027, 2008.

Lai, W., Pan, J., Devlin, A. T.: Impact of tides and winds on estuarine circulation in the Pearl River Estuary. *Continental Shelf Research*, 168, 68-82. doi: 10.1016/j.csr.2018.09.004, 2018.

**Point 2: Not enough information is given regarding the wave model parameters. Please give details on how the wave radiation stresses are calculated in the model and how the waves are incorporated in the model equations i.e., via the mentioned JONSWAP spectrum, the frequency of occurrence of different wave heights and directions and number of days in different seasons and the wave fixed parameters at the open boundary (lines 295-300).**

Response: We have now included detailed information about the wave model parameters and how wave radiation stresses are calculated. The wave model employed in this study is the open-source Simulating WAVes Nearshore (SWAN) model, which is widely recognized for its accuracy in wave action calculations.

The wave radiation stresses in the SWAN model are computed by solving the wave action conservation equation, taking into account wave nonlinearity and spectral peak shifting. At the

open boundaries, we have set up the model using the JONSWAP spectrum, which is a well-established spectrum for representing the statistical properties of wind-generated waves in deep water. The specific parameters for the JONSWAP spectrum have been added in the appropriate section of the manuscript. To ensure the accuracy of the wave boundary conditions, we have adjusted the parameters based on multi-year wave data from the Dongfang Station. The directional resolution is set to 40 sectors, with a particular focus on the southwest (SSW) and southwest (SW) directions where the waves are most frequent.

The revised sentence now reads as follows:

*“Considering the limitations of the FVCOM model in wave calculations, this study selects the widely-used third-generation SWAN model (SWAN team, 2006) for numerical simulation of wind waves in this region. The wave field are driven by wind and current from hydrodynamic model. The parameters used in the model setups are based on the values listed in Table 6. The wave model at the open boundary is defined by the JONSWAP spectrum, with a spectral resolution of 40 frequency bins and 36 directional sectors. Calibrate the parameters using multi-year wave data from the Dongfang Ocean Station. The directional resolution is set to 40 sectors, with a particular focus on the southwest (SSW) and southwest (SW) directions where the waves are most frequent. The wind speed and wind direction are from the ERA5 reanalysis data provided by ECMWF. The peak parameter ( $\gamma$ ) of the JONSWAP spectrum, indicative of the wave asymmetry, was specified at 3.3, and the spectral width parameter was set to 0.07 to define the shape of the wave spectrum.*

**Table 6** Parameters of the wave model

Parameter	Value
Whitecapping dissipation ( $C_{ds}$ )	$2.36 \times 10^{-5}$
Pierson–Moskowitz ( $S_{pm}$ )	$3.02 \times 10^{-5}$
Dissipation (alpha)	1.0
Breaking index (gamma)	0.73
JONSWAP formulation ( $C_{bottom}$ )	0.067

”

**Point 3: Although the simulation period is never explicitly mentioned in the manuscript, it seems that this coincides with the calibration period (23/04-30/04/2023). To be validated though, the model needs to run with the same setup for another period. In addition, there is no mention in the manuscript of the calibration parameters (e.g., roughness, diffusion, viscosity etc.) and how these were modified. For example, do the authors use uniform values or spatially varying ones?**

Response: Thank you for your insightful comment regarding the calibration parameters and the simulation period of our model. In response to your feedback, we have now included a comprehensive description of the calibration parameters in our manuscript. The calibration is performed using water level data from the Basuo Port from April and May of 2022. We have added a new table in the "Model Region and Settings" chapter, where we detail the calibration parameters such as roughness, diffusion, and viscosity. These parameters were adjusted using the control variable method, which involves a systematic approach to modify one parameter at a time while keeping others constant to observe and quantify its impact on the model output.

The revised sentence now reads as follows:

*“In this study, we calibrated the hydrodynamic model using water level data from April and May of 2022. The data were collected from Basuo port station. One-At-a-Time (OAT/OFAT) method (Czitrom, 1999) is used to modify the parameters, an effective local sensitivity analysis technique. In each experiment, we alter one factors while holding the others constant. During the calibration process, our primary focus was on the model's hydrodynamic response. This was achieved by adjusting the flow resistance parameters and the bed roughness coefficients within the model. The calibrated model parameters are presented in Table 5.*

Table 5 Parameters of the hydrodynamic model

Parameter	Value
Shoreline	GSHHS

Bathymetry	ETOPO1 and ADCP in-situ
Grid	0.25 km at the boundaries to 25 m near the coastline
Time period	23/4/2023 00:00-30/4/2023 00:00 (Spring neap tide) 28/6/2022 00:00-1/8/2022 00:00 (High water period)
Manning number	28
Eddy viscosity	Smagorinsky formulation data 0.28 m <sup>2</sup> /s
Time step	300 s
Tidal constituents	M2, S2, K1, O1, N2, K2, P1, Q1
Wind/Sea level Pressure	ERA 5
Validation	Basuo Port Station (19°06' N, 108°37' E) ADCP 01, ADCP 02

---

”

**Point 4: The model grid is not presented, is it structured or unstructured? Is it regular or curvilinear? What is the model’s resolution? The limits of the white rectangular in Figure 6 do not coincide with the grid coordinates as given in Line 280. The authors claim in lines 286-289 that the resolution of the ETOPO1 data is not sufficient for this research however it seems that these are the data used for developing the bathymetry of their model as it is written in the legend of Figure 6. The time step is also missing.**

**Response:** We sincerely apologize for the oversight regarding the model grid details and the associated errors in Figure 6. Your feedback is invaluable, and we have taken immediate steps to rectify these issues and enhance the clarity of our manuscript.

**Model Grid Details:** We have now included a detailed description of the model grid in the "Model Region and Configuration" section of the manuscript. The Finite Volume Coastal Ocean Model (FVCOM) utilizes a non-structured triangular grid, which allows for flexible resolution and better adaptation to complex coastal geometries. The specific details of the grid, including the number of nodes and elements, are as follows:

- Grid Type: Unstructured triangular grid
- Number of Nodes: 13,814

- **Resolution:** In the offshore region, the grid density is lower, with a resolution of 0.25 km, while the nearshore part of the open boundary has higher grid resolution. In the main research area near the river channel, the grid resolution is highest, reaching 25 m.

The model's resolution varies from 14 minutes to 7 minutes, with higher resolution in the area of interest to capture the detailed coastal dynamics. The grid is refined near the coast and in the estuary to better resolve the complex flow patterns and sediment transport processes.

**Correction of Figure 6:** We have revised Figure 6 to accurately represent the model grid and its boundaries. The white rectangular limits now correctly coincide with the grid coordinates, providing a clear visual representation of the model domain and its spatial extent.

**ETOPO1 Data Clarification:** We acknowledge the confusion caused by the previous description of the ETOPO1 data usage. The ETOPO1 data, with a resolution of 1 arc-minute, was indeed used as a base to develop the bathymetry of our model. However, the scope of the model is small. The model's span is 14 arc-minutes by 7 arc-minutes. Therefore, we have conducted topographic surveys using an ADCP-equipped survey vessel. The measured data have been interpolated to generate the high-resolution terrain information used in our model. The specific locations of these survey points are now clearly indicated in Figure 6.

**Model Time Step:** The model was run with a time step of 300 seconds, which is suitable for capturing the rapid changes in water levels and currents in the coastal area.

The revised sentence now reads as follows:

*“..., The model employs a triangular unstructured grid. To enhance computational accuracy and reduce computation time, the density of boundary nodes gradually decreases from nearshore to offshore. In the offshore region, the grid density is lower, with a resolution of 0.25 km, while the nearshore part of the open boundary has higher grid resolution. In the main research area near the river channel, the grid resolution is highest, reaching 25 m. The entire study area grid comprises a total of 13, 814 computational nodes.....”*

The revised figure now shows as follows:

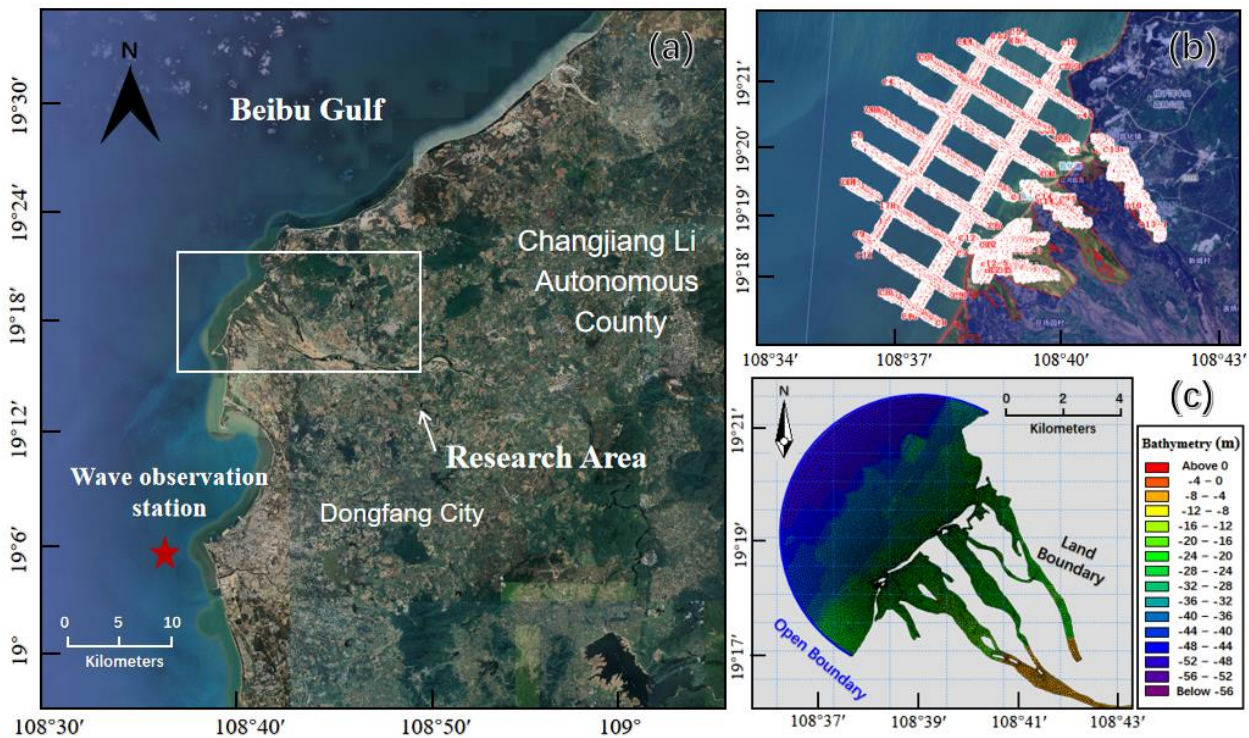


Figure 6 (a) Scope of study area (the white frame) and wave observation (the red star) from Dongfang; (b) ADCP collection points on site; (c) Grids and boundaries (map origination: <https://hainan.tianditu.gov.cn/>)

**Point 5:** The hydrodynamic results (section 3.3) are ill-presented and not adequately analysed. At which moment the results given in Figure 9 correspond to? Are these depth and/or time averaged? The depicted current of Figure 9 is in some instances referred to as a tidal (line 345) and in others as a coastal one (line 430). Are these averaged, combined tide and wave currents over this week of simulation or are taken at a certain time of calculation and if so, which one? Furthermore, it is written that the results are given at the times of high and low water but tidal currents at these times are minimal. What's the situation at slack times? Finally, there is no mention in the manuscript of whether we are looking at a period of neap or spring tide. Water levels in Figure 7 remain almost constant during the simulation period and in any case a spring-neap cycle takes place within 15 days and not one week (lines 473-478).

Response: We have taken your comments seriously and have made substantial revisions to address the concerns raised regarding the hydrodynamic results presentation and analysis.

**Clarification on the Timing of Results:** We acknowledge the lack of clarity regarding the

timing of the results presented in Figure 9. We have now specified that Figure 9 corresponds to the peak flow moments during both ebb and flood tide cycles, which occur at the transition phases between high and low tide. The revised part now reads as follows:

*“..., Figure 10b and 10c depict the flow field outside the estuary of the Changhua River. Figure 10b shows the flow field at 23:00 on April 23, 2023, corresponding to the peak of the flood tide (Rapid flooding tide). At this time, the tidal current flows in a northeast direction with a maximum speed of 0.62 m/s. Figure 10c shows the flow field at 13:30 on April 24, 2023, corresponding to the peak of the ebb tide (Rapid ebb tide), where the tidal current flows in a southwest direction with a maximum speed of 0.75 m/s. Overall, the tidal currents outside the Changhua River estuary generally follow a northeast-southwest reciprocating pattern, with flood tides flowing northeast and ebb tides flowing southwest, parallel to the shoreline. The maximum ebb current is faster than the maximum flood current.”*

**Depth and Time Averaging:** The depicted currents in Figure 9 are indeed instantaneous but not time and depth averaged over the simulation period.

**Tidal Currents Distinction:** We have revised the manuscript to distinguish clearly between tidal and coastal currents. The revised sentence now reads as follows:

*“..., The predominant northeast-southwest **tidal** current direction and wave action, has led to the formation of a two-way sand mouth, further narrowing the estuary....”*

**Simulation Period and Neap-Spring Tide Cycle:** The study area experienced an incomplete transition from a new moon to the first quarter moon between April 22, 2023, and April 27, 2023. During the new moon, a spring tide occurred, and during the last quarter moon, a neap tide occurred. This is not the 15-day spring-neap cycle in the strict sense. The spring-neap cycle refers to the period from one spring tide to the next spring tide, or from one neap tide to the next neap tide. Since April 22, 2023 (the third day of the lunar month) was during the new moon, it was the last day of the period of spring tide. April 27, 2023 (the eighth day of the lunar month) fell during the first quarter moon, hence the transition from spring tide to neap tide as described.

The added part (section 3.3) now reads as follows:

“Figures 11a and 11b illustrate the flow field inside the estuary of the Changhua River. Figure 11a shows the flow field at 23:00 on April 23, 2023, corresponding to the peak of the flood tide. Inside Estuary A, due to the topography, a large counterclockwise circulation forms around the central island, accompanied by several smaller vortices, with the overall trend of tidal currents flowing southeast along the river channel. In Estuary B, ocean inflows meet with river flows from upstream, ultimately converging into Estuary C through the passage between B and C. In Estuary C, the flow is more unidirectional compared to A and B, with upstream water flowing into the ocean, then following the northeast-directed tidal current outside the Changhua River estuary. Figure 11b shows the flow field at 13:30 on April 24, 2023, at the peak of the ebb tide. At this time, the circulation inside Estuary A reverses to a clockwise direction, and other smaller vortices change direction accordingly, with the overall trend of tidal currents flowing from upstream to the ocean. In Estuary B, the dominant force is the high-speed flow from Estuary C, which enters B through the narrow passage between B and C, splitting into two opposite directions: one part flows into the ocean, and the other flows upstream, forming a circulation within the river channel. In Estuary C, the water flows upstream from the ocean along the river channel.

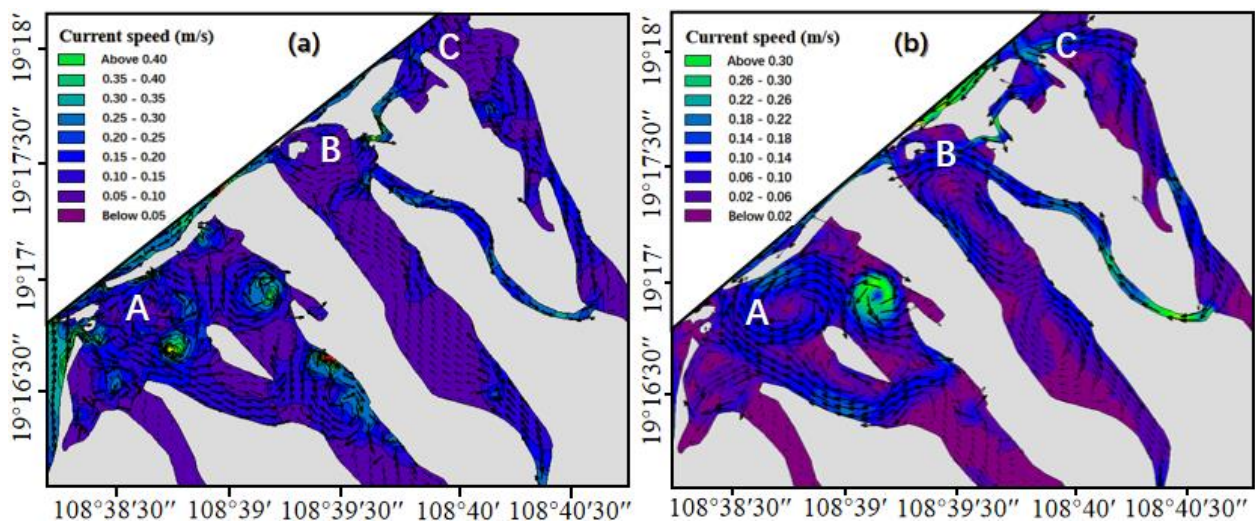


Figure 11 Flow field inside the estuary : (a) moment of the maximum flood current; (b) moment of the maximum ebb current

*To further analyze the characteristics of the flow field in the study area, flow fields are selected for analysis during the transition from low tide to high tide and from high tide to low tide. Figure 12f depicts the location of the research area. Figure 12a shows the flow field at low tide, where the tidal current outside the estuary flows northeast, and water in the main river channel downstream of the Changhua River flows upstream from the ocean. After low tide (during flood tide), water flow velocity gradually increases, with the tidal current outside the estuary consistently flowing northeast. During this period, the main river channel maintains an eastward flow.*

*Figure 12b illustrates the moment of flow direction change during flood tide, when the flow direction outside the estuary rotates clockwise along the shoreline from the south (toward Beili Bay). The northern ocean current (outside Changhua Harbor) also begins to rotate clockwise, flowing into Estuary C, then into the ocean through the passage between B and C, forming a circulation that enhances the clockwise rotation of the northern ocean current. Subsequently, the flow direction gradually changes from northeast to southwest as it moves from the coast toward the open sea. The sand spit at the downstream estuary alters the flow direction and velocity. The sand spit can act as a natural barrier, causing the tidal current to change direction earlier during flood tide.*

*Figure 12c shows the flow field at high tide, where the tidal current outside the estuary has fully shifted to the southwest, while the flow direction further offshore is still transitioning. In the main river channel, the water flows from upstream toward the ocean. Estuaries B and C are influenced by the coastal current outside the northern part of the study area, flowing into the estuary opposite to Estuary A. After high tide (during ebb tide), the water flow velocity in the study area gradually increases, with the tidal current outside the estuary consistently flowing southwest. After some time, the water currents in the southern and northern parts of*

*the study area turn counterclockwise, and the flow direction in the B and C channels changes from inward to outward.*

*Figure 12d shows the flow field at the moment when the flow direction changes during ebb tide. It is evident that there are two counterclockwise circulations outside the Changhua River estuary: one from Beili Bay and the other from outside Changhua Harbor. The latter has a broader influence and thus plays a dominant role in determining the water flow direction in the study area, gradually shifting the coastal current from southwest to northeast. Figure 12e shows the flow field at low tide once again, where the water flow outside the estuary has shifted back to the northeast, repeating the previous flow pattern.*

*In summary, during the transition from flood to ebb tide, the flow field outside the estuary is driven by the deflection of water currents from Beili Bay and Changhua Port, shifting the flow direction from northeast to southwest. During the transition from ebb to flood tide, the deflection is primarily influenced by the circulation outside Changhua Port, shifting the flow direction from southwest to northeast. In channels A, B, and C within the study area, the flow direction changes are relatively consistent due to the passage between B and C. The flow direction in channel A aligns with the main river channel, flowing inward during flood tide and outward toward the ocean during ebb tide.*

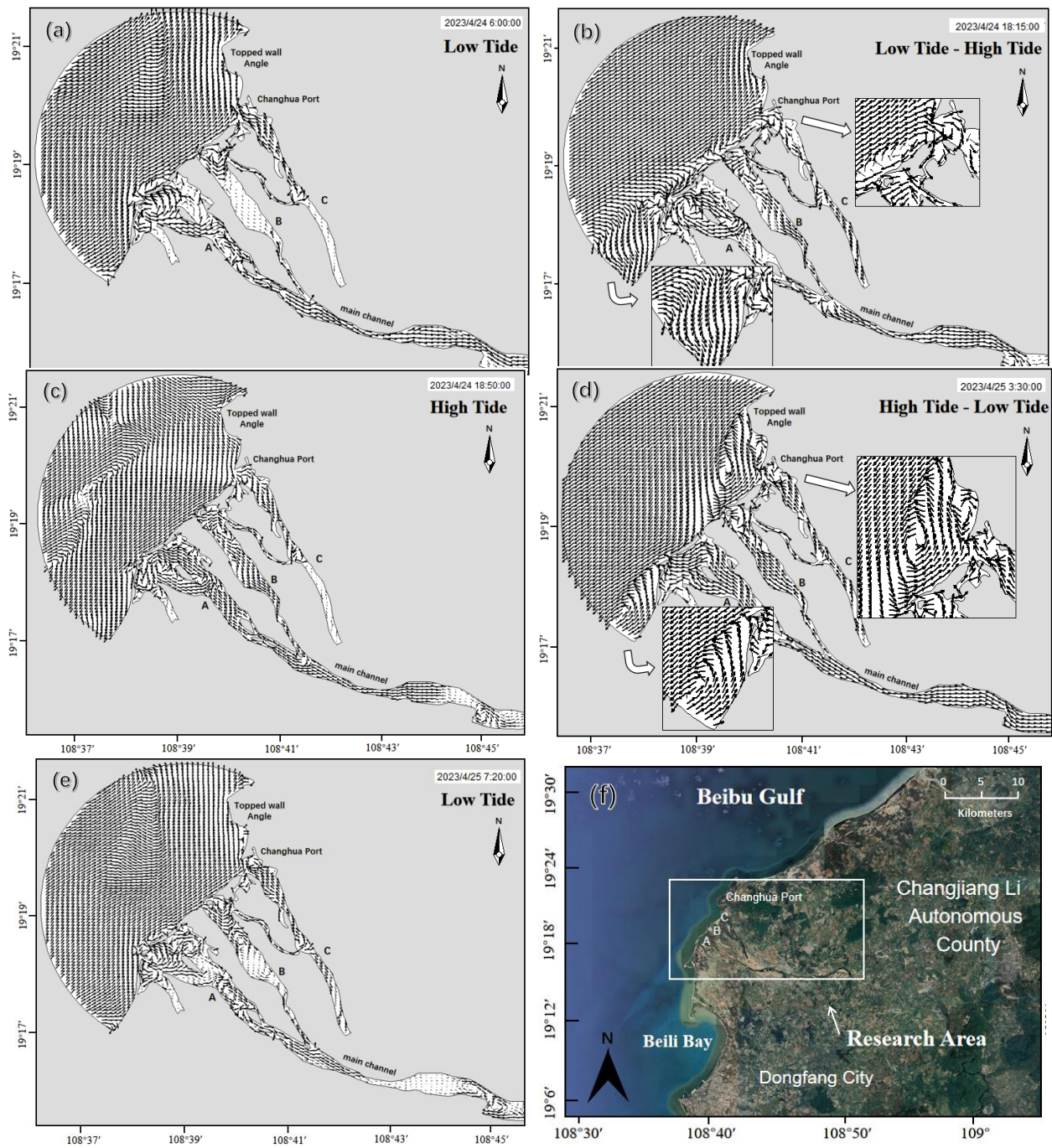


Figure 12 Transition of the flow field (a-e) and location of the study area (f)

”

**Point 6:** The authors underline the fact that the tide is the most prominent effect at the point of comparison against wind and waves (lines 335-336) but under these

circumstances, their validation process cannot be considered as a validation of the combined effect of current-wave but only of tide. Therefore, a case where all factors are important is required to demonstrate the relative capability of the model.

Response: We sincerely apologize for the analysis error here. I have revised the description here, and the verification here is the verification of the hydrodynamic model.

The revised part now reads as follows:

*“. The proximity of measurement point ADCP 01 to the land, coupled with its relatively shallow water depth, results in sea water being more susceptible to obstruction by the topography and friction from the seafloor at this location....”*

**Point 7: The manuscript misses information on the initial and boundary conditions and rates for both bed load and suspended sediments transport. The sediment motion equation implemented in the model (line 363) needs to be presented. How are the two modules coupled? Is it an online or offline coupling?**

Response: Thank you for your insightful comments and suggestions regarding the sediment transport model in our manuscript. We have taken your feedback seriously and have made the following revisions to address the concerns raised:

**Initial and Boundary Conditions:** We have now included detailed information on the initial and boundary conditions in Section 2.1 of the manuscript. The initial conditions for sediment concentration and the boundary conditions, including the influx of sediment at the upstream boundary, have been explicitly defined. The revised part now reads as follows:

*“. The upstream boundary is assigned a flow rate of 44 m<sup>3</sup>/s, and the suspended sediment concentration is set at 5 g/m<sup>3</sup>. The median grain size and sorting coefficient of the initial sediment distribution are determined through the partitioning based on the measured sediment data from Section 2.3. The porosity is set to 0.4, and the sediment density is 2650 kg/m<sup>3</sup>....”*

**Sediment Transport Equations:** We have presented the equations of bed load and suspended load transport rate, which are crucial for understanding the model's approach to sediment dynamics. The equations are show as follow:

$$q_s = f_{sl} \cdot C_a \cdot u_*^2 \quad (5)$$

$$q_b = 0.053 \frac{M^{2.1}}{D_*^{0.3}} \sqrt{(s-1)g \cdot d_{50}^3} \quad (6)$$

Where  $q_b$  is the bed load transport rate;  $q_s$  is the suspended load transport rate;  $M$  is the non-dimensional transport stage parameter;  $u_{f,c}$  is the critical friction velocity, which under the current;  $\theta_c$  is the critical Shield parameter;  $u_{f,e}$  is the effective friction velocity;  $C'$  is the Chezy number originationg from skin friction;  $D_*$  is the non-dimensional particle parameter;  $\nu$  is the kinematic viscosity and approximately equal to  $10^{-6}$  m<sup>2</sup>/s for water;  $C_a$  is the bed concentration;  $u_*$  is the friction velocity;  $\tau$  is the shear stress at the bed surface;  $\rho$  is the density of water;  $m$  is empirical exponent.”

**Coupling of Modules:** We have clarified that the coupling between the hydrodynamic and sediment transport modules is performed offline. The detailed part now reads as follows:

“A mathematical model established through a wave-current coupling approach can accurately describe the motion laws of wave-generated currents and consider the impact of nearshore currents on wave propagation. It also reflects the interaction between nearshore waves and currents. In this paper, a three-dimensional sediment transport model is constructed using the model coupler MCT to perform real-time coupling between the hydrodynamic model FVCOM and the wave model SWAN, employing the same unstructured grid for the coupling (Chen et al., 2018; Ji et al., 2022). The coupling process can be summarized as follows: the FVCOM hydrodynamic model and the SWAN wave model transmit the calculated three-dimensional flow field and wave data to the sediment module, which then calculates the suspended and bed

*load sediment transport rates, achieving data linkage between the three-dimensional wave-current coupled model and the sediment transport model.”*

**Revision of Line 363:** We apologize for the confusion caused by the previous description. After careful consideration, the part in this section has been deleted.

**Point 8: As mentioned earlier, the model’s given equations (1)-(4) in the paper are two-dimensional depth averaged. How is then the velocity vertical profile computed in equation (7)?**

Response: Thank you for your comment regarding the clarification needed on the model's velocity vertical profile computation. We acknowledge the mistake in the initial presentation of the model equations and appreciate your guidance on this matter. In response to your feedback, we have removed the incorrect Equations (1)-(4) that were mistakenly presented as two-dimensional depth-averaged. FVCOM model is an open source model, its control equation and introduction can be found in the link of data availability behind the conclusion of this paper.

**Point 9: The authors calculate a uniform over space sediment thickness from their model equal to 4.1 cm. If what they write in lines 365-366 is right, then they get results after the one-week simulation that they did for 23/04/2023-30/04/2023. But then they use the estuary’s sediment discharge of 2022 (line 389-390) and they compare their model result with field data covering one month (July 2022)!! Not surprisingly then, there is a serious discrepancy of 1.1 cm between the model and the observations which is too big to be ignored. Besides, the assumption that the uniform over space result from a one-week simulation for a certain year can be representative of any year for that specific area is too crude.**

Response: Thank you for pointing out the need for clarity on the sediment transport calculations within our model. In response to your comments, we have decided to remove the section that may cause further misunderstanding. We have removed the theoretical validation section, leaving only the validation part based on measured data (Section 5.1, where we presented the comparison of observed and simulated suspended sediment concentration (SSC) data at the Baoqiao Station in the lower reaches of the Changhua River.). The result of empirical validation is as follows:

*“In the lower reaches of the Changhua River, the summer season is the most pronounced for sediment variation within a year, with the highest sediment concentration and sediment transport rate (Mao et al., 2006). Therefore, sediment data from July, which is representative, are selected for model validation. The simulated Suspended Sediment Concentration (SSC) is compared with the daily observed SSC at Baoqiao Station for the month of July (Figure 13). The SSC at Baoqiao Station is the highest during the first two days of July, reaching a peak SSC of 0.55 kg/m<sup>3</sup>. Subsequently, the SSC continuously decreases, reaching its lowest value on the 5th of July, and then slowly rises. After the 10th of July, it gradually decreases from 0.301 kg/m<sup>3</sup>, with the most values remaining below 0.2 kg/m<sup>3</sup>. Based on the analysis, NSE for Baoqiao Station is 0.8389; the RMSE is 0.097244 kg/m<sup>3</sup>. The observed SSC are in good agreement with the simulated values.*

*To further analyze the simulation validation, Figure 13 presents a histogram of the daily absolute error in SSC at Baoqiao Station. The absolute error is calculated as the absolute difference between the measured and simulated values. The Mean Absolute Error (MAE) is defined as the average over the test sample of the absolute differences between prediction and actual observation. The MAE in SSC for Baoqiao Station in July is 0.071224 kg/m<sup>3</sup>. The maximum error occurs at the beginning and the end of the month, which may be due to the use of monthly average flow and sediment data for the model's upper boundary input, thereby increasing the model's error. Overall, the difference between*

the daily observed SSC values and the simulated results at Baoqiao Station in July is within a reasonable range, indicating that the model has an acceptable level of precision.

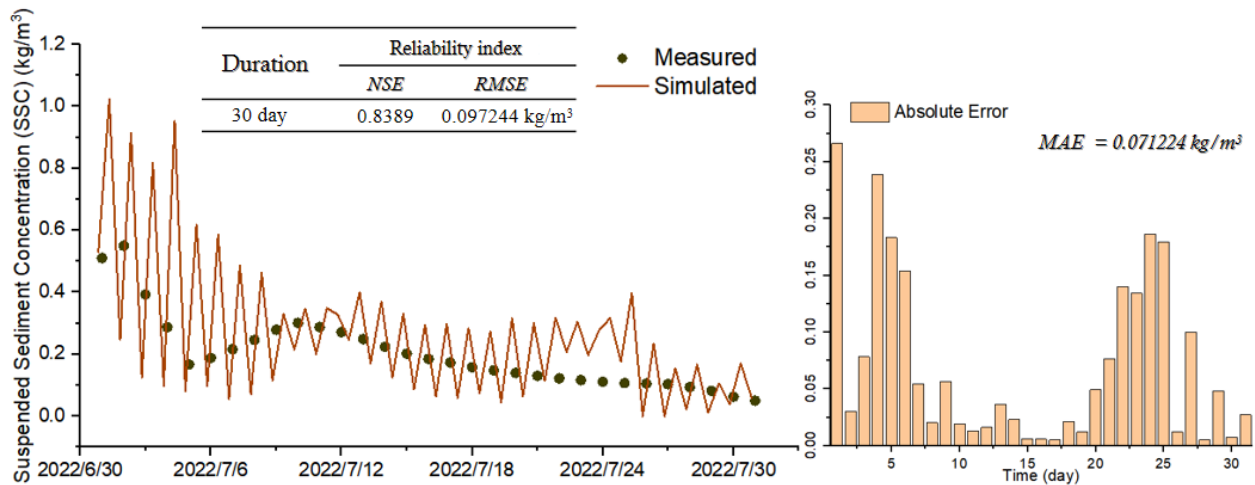


Figure 13 Selection point for sediment deposition verification ”

**Point 10:** From what is written in section 3.4.2, it seems that the authors not only have sediment data for an entire month (July 2022) but that they run their model for this period as well. Why don't they do then the comparison based on results from this simulation? In any case, the fact that they present results analysis for different time periods is already problematic.

**Response:** Upon reflection and in response to your feedback, we have decided to focus solely on the validation of the sediment transport model using the daily sediment concentration data from July 2022. Initially, these data were not available to us, which led to our reliance on a preliminary theoretical validation approach. Therefore, after we obtained the actual field measurements, we included both the theoretical and empirical validation methods in our manuscript. We recognize that presenting analyses from different time periods could potentially confuse readers and affect the overall coherence of our study. Therefore, we have revised the manuscript to remove the earlier theoretical validation and now present a

comprehensive validation based on the July 2022 data. This revision ensures that our model validation is grounded in actual field observations, enhancing the reliability and relevance of our findings. The detailed part now shows in Section 5.1 (Response in Point 9)

**Point 11: In their figures, the authors fail to provide all the necessary information regarding their study case. They refer to stations that can be nowhere found in their figures and so the reader cannot understand from which location the results and data are taken? Specifically, Dongfang Ocean station, Danchangcun, Xiantiancun and Jiuxiancun stations cannot be found in the figures. The same for the ADCP.**

**Response:** We appreciate your feedback regarding the clarity and comprehensiveness of our figures and the corresponding descriptions in the manuscript. We understand the importance of providing detailed and accurate geographical information to ensure the reader's full comprehension of our study. In response to your comments, we have now included detailed maps with clear labeling of all the stations mentioned, including Dongfang Ocean station, Danchangcun, Xiantiancun, and Jiuxiancun, as well as the ADCP locations. These maps are incorporated into the relevant sections of the manuscript and are referenced within the text to guide the reader.

The added and revised figures now show as follows:

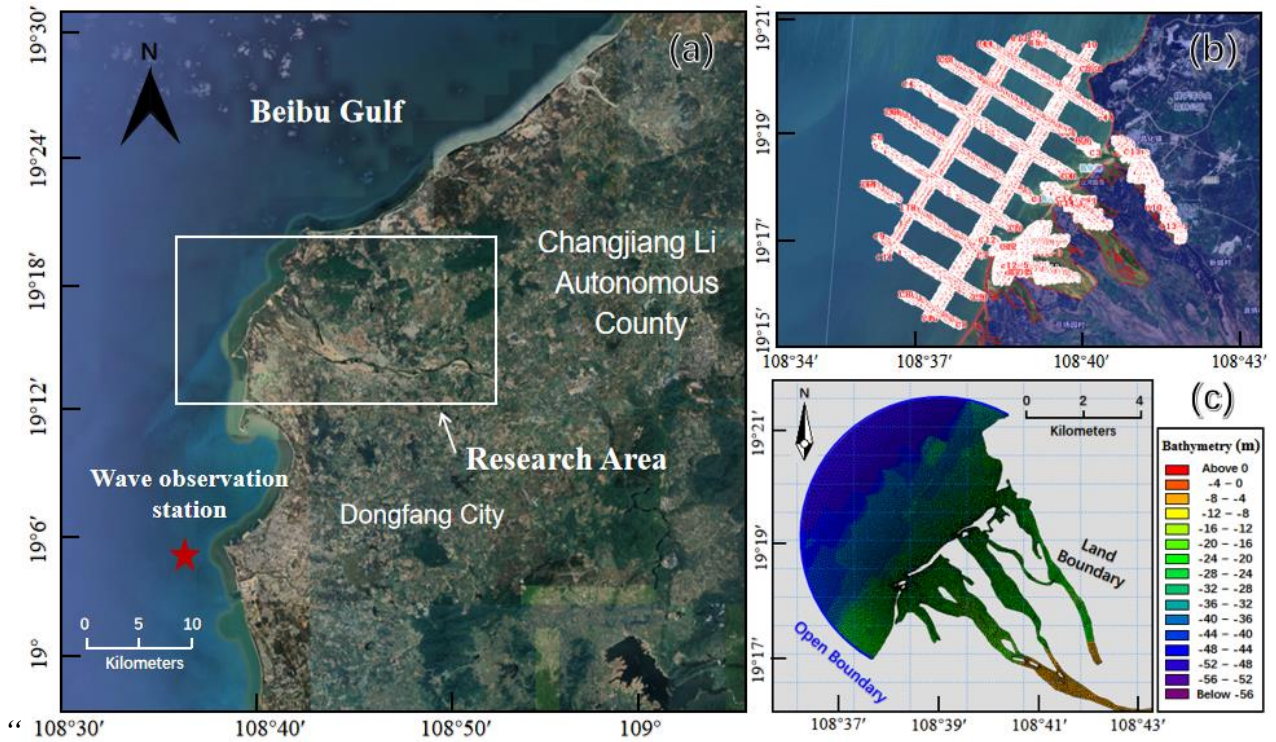


Figure 6 (a) Scope of study area (the white frame) and wave observation (the red star) from Dongfang; (b) ADCP collection points on site; (c) Grids and boundaries (map origination: <https://hainan.tianditu.gov.cn/>)

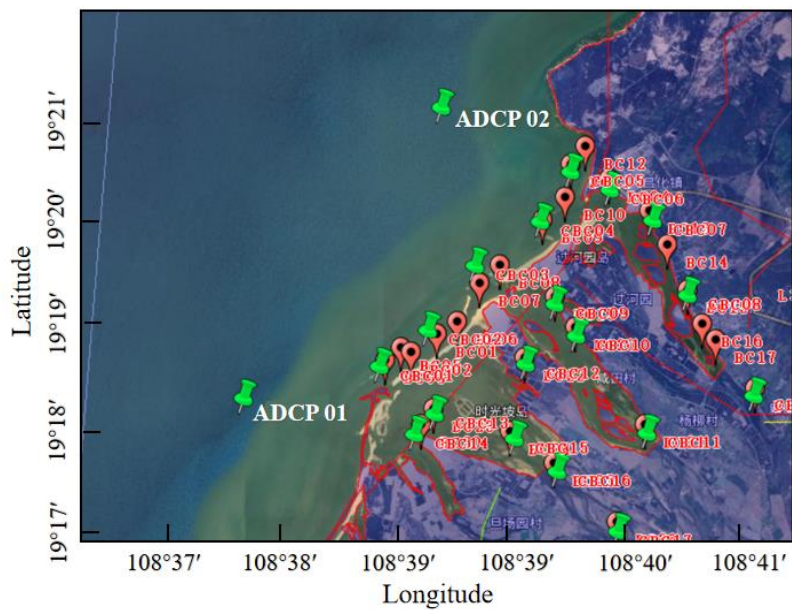


Figure 8 Specific location of ADCP

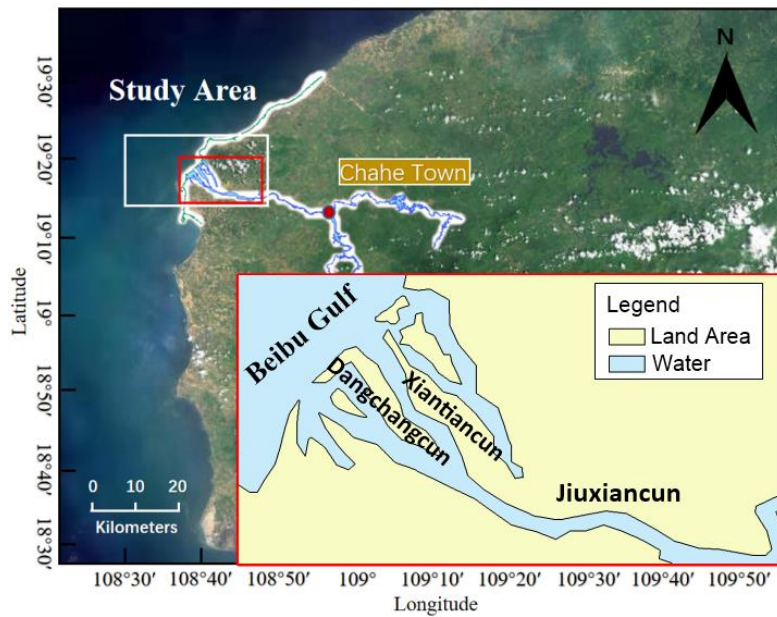


Figure 14 Information of important place names in simulated areas

”

**Point 12: Chapter 4 does not discuss the scientific output and fails to explore and highlight the importance of the outcomes. It only provides a list of potential measures to be taken against siltation which have only a local interest. These can be hardly supported considering that they are based on conclusions from not adequately justified modelling. I suggest that the authors rewrite this section after they have addressed all the raised issues in their modelling approach but from a non-local perspective.**

Response: Thank you for your constructive criticism regarding Chapter 4 of our manuscript. We have taken your suggestions to heart and have completely revised the chapter to provide a more comprehensive perspective on the significance of our findings. In the updated Chapter 4, we have expanded our discussion to delve into the critical role of residual currents in sediment transport. Our analysis now includes a comparative examination of the behavior of residual currents during low and high water periods, offering insights into their varying influence on sediment dynamics across different environmental conditions.

The rewritten Chapter4 now reads as follows:

## **“6. Discussion**

### **6.1 Residual Current**

*Residual currents to some extent reflect the transfer and exchange of water bodies, and their direction is usually the direction of sediment movement and the dispersion and migration of pollutant substances (Robinson, 1983). They are closely related to the long-term transfer and deposition of estuarine materials. Therefore, studying the characteristics of residual currents in this sea area under the combined action of waves and currents can comprehensively understand the evolution characteristics of the sea area's sediment. Tidal residual currents can be studied using the Lagrangian and Eulerian methods. Eulerian residual current refers to the average transfer caused by the average flow after removing the periodic astronomical tide, and its magnitude and direction mainly depend on the strength and duration of the ebb and flood tidal velocities within the tidal cycle; Stokes' drift characterizes the net drift of the water body, and its numerical size directly reflects the correlation between the tidal range and the change in flow velocity within the tidal cycle, and the sum of the two is the Lagrangian residual current. The Lagrangian residual current is not the result of the long-term tracking of real particles, but is the result of the superposition of Eulerian residual current and Stokes' drift.*

*Eulerian residual current refers to the average transfer caused by the average flow after removing the periodic astronomical tide, and its magnitude and direction mainly depend on the strength and duration of the ebb and flood tidal velocities within the tidal cycle; Stokes' drift characterizes the net drift of the water body, and its numerical size directly reflects the correlation between the tidal range and the change in flow velocity within the tidal cycle, and the sum of the two is the Lagrangian residual current. The formulas for calculating Eulerian*

residual current and Stokes' drift refer to previous studies (Longuet-Higgins, 1969; Uncles and Jordan, 1980; Li and O'Donnell, 1997).

Through the analysis of sediment simulation results from the previous section on the distribution of major sedimentation areas, we have been able to understand the distribution of these areas. However, the causes of sedimentation require further exploration. In this section, based on the tidal current field data from hydrodynamic numerical simulation, we calculate the residual flow according to the entire study area. The flow velocity measured data from two ADCP stations outside the estuary of the Changhua River was analyzed using the tidal residual current calculation method, thereby enhancing the credibility of the residual flow field.

**Table 8** Residual currents in spring neap tide at each station

Station	Eulerian residual current		Stokes' drift		Lagrangian residual current	
	Speed (m/s)	Degree (°)	Speed (m/s)	Degree (°)	Speed (m/s)	Degree (°)
ADCP01	0.0913	232	0.0006	172	0.0917	231
ADCP02	0.0331	137	0.0007	194	0.0335	138

The Lagrangian residual current at monitoring station ADCP01 is 0.0913 m/s with a direction of 231° (SW), and at station ADCP02 it is 0.0331 m/s with a direction of 138° (NW) (Table 8). In the area outside the Changhua River estuary, the Stokes tidal residual current at the monitoring stations is two orders of magnitude smaller than the Eulerian residual current. Therefore, the flow trend of the composite Lagrangian tidal residual current remains essentially consistent with that of the Eulerian residual current.

## 6.2 Influence of residual current in low water period

The study area has a distinct monsoon climate, with prevailing southerly winds in the summer and alternating southerly and northeasterly winds in the spring. The figure 20 shows the Eulerian residual current field during the simulation period (low water period). To present

*the Eulerian residual currents within the study area in a complete and clear manner; a limit on vector length was set when plotting the current field. Consequently, the direction and length of the arrows in the figure represent the direction of the residual currents, but not their intensity. However, the intensity of the Eulerian residual currents can still be discerned through the data at the grid points. The Eulerian residual current outside the Changhua River estuary generally flows southward. As it flows from north to south, it is obstructed by the sand spit, diverging around it. After the divergence, the southwestward Eulerian residual current splits, with one part following the sand spit to the river mouth near A, and the other part entering channel B and flowing inward. The northeastward Eulerian residual current, after divergence, encounters the obstruction of the headland (Topped wall Angle) and forms a counterclockwise circulation below Junbi Jiao. Headlands are one of the key topographical features where strong residual current vortices occur (Maddock et al., 1978; Pingree et al., 1977; Smith, 2010). At the headland, the water depth shoals in the onshore direction, and the frictional effect is stronger in shallow water areas than in deep water areas. This results in a frictional force moment on the alongshore tidal current, generating vorticity. The transport of vorticity within the closed circulation lines on either side of the headland is not equal in input and output. After a tidal cycle of time averaging, a net vorticity will be produced on both sides of the headland, forming two counter-rotating residual current vortices, with the tidal residual current at the tip of the headland generally pointing seaward (Zimmerman, 1981). Topped wall Angle, being a headland, can produce similar residual current field results. A clockwise residual current vortex opposite to the one below may exist above Topped wall Angle. The Eulerian residual currents in the three river channels where A, B, and C are located all flow towards the river mouths. The Eulerian residual current in the channel between B and C flows from B to C.*

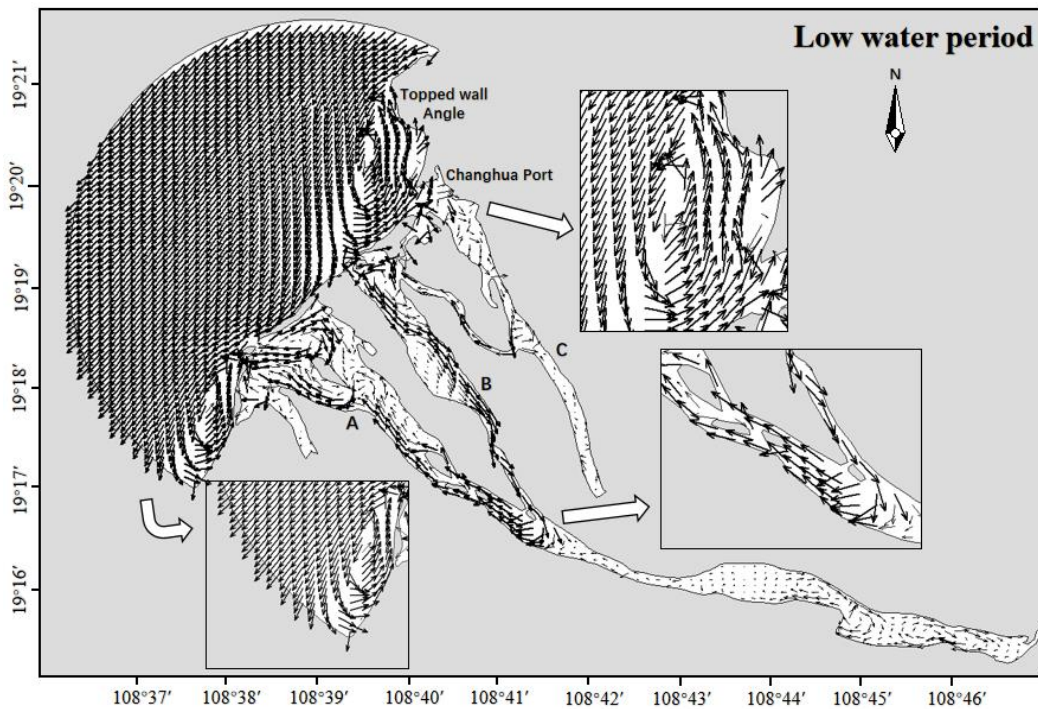


Figure 20 Eulerian residual current field during low water period

### 6.3 Influence of residual current in high water period

*In order to comprehensively understand the residual current field of the study area, it is essential to analyze the residual current field during the flood season. The figure displays the Eulerian residual current field of the study area for July 2022 (high water period). The Eulerian residual current south of the river mouth in the study area still flows to the south (towards Beili Bay), but the nearshore residual current veers more quickly, resulting in a smaller circulation compared to the dry season. The circulation range in the north has expanded, likely due to the influence of the southerly monsoon during the summer, leading to an increase in the strength and directional deflection of the Eulerian residual current. When it reaches the shore, it is naturally obstructed by the sand spit and disperses to both sides (NE-SW). The upward Eulerian residual current, upon encountering the sea area outside Changhua Port, is deflected by the coastal promontory (Topped wall Angle) and turns westward. The westward Eulerian residual current, continuously affected by the strong southerly winds during*

its movement, keeps deflecting. Eventually, a circulation is formed, with a circulation range larger than that of the dry season. The situation in channel A is essentially consistent with the dry season, while the Eulerian residual current directions in channel B and C are the same as that in A, all flowing towards the ocean. This is quite different from the dry season, with a flow direction opposite to that of the dry season, which may be related to the increased rainfall and subsequent increase in downstream flow during the summer flood season.

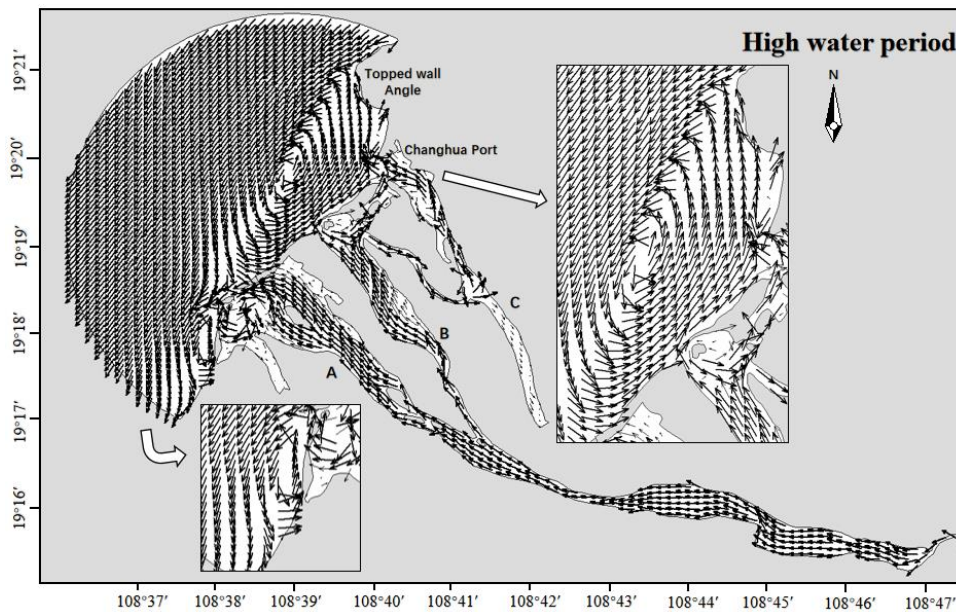


Figure 21 Eulerian residual current field during high water period

”

**Point 13: The conclusions read more like a summary. What are the key findings of this research, which messages can we take from this and why these would contribute further to the research on this topic?**

Response: providing a comprehensive and transparent description of how the data can be accessed. Thank you for your insightful feedback on our manuscript's conclusion section. We have taken your comments seriously and have reworked the conclusion.

The revised conclusion now reads as follows:

*“The study successfully applied a wave-current coupled sediment transport model to the lower reaches of the Changhua River in Hainan Island. By integrating field measurements, remote sensing techniques, and the Van Rijn model, this research has developed a comprehensive model capable of accurately simulating sediment behavior under the combined action of waves and currents. The following conclusions reflect a robust understanding of the study's themes:*

*The study area's surface sediments consist of ten types, including gravelly sand, sandy gravel, silty gravel, sandy silt, silt, gravelly silt, sand, gravelly sandy silt, gravelly sand, and silty gravelly sand. Among these, gravelly sand and gravelly sand are the predominant types.*

*During the transition from flood to ebb tide, the flow field outside the estuary is driven by the deflection of water currents from Beili Bay and Changhua Port, shifting the flow direction from northeast to southwest. During the transition from ebb to flood tide, the deflection is primarily influenced by the circulation outside Changhua Port, shifting the flow direction from southwest to northeast.*

*The main sedimentation areas within the study area's river channels include Xiantiacun, Danchangcun, and Jiuxiancun. The first two experience sediment deposition near the river mouth's sand spit, while the latter's sediment is primarily deposited near the river bifurcation.*

*Regardless of whether it is the dry season or the flood season, the residual currents in the study area are directed towards Beili Bay (SWS), implying that sediments in the lower reaches of the Changhua River will be influenced by the residual currents and transported towards Beili Bay. The sand spit at the river mouth, affected by the southward residual currents, will cause sediments from the north to be transported towards the northeast and southwest of the sand spit, leading to its elongation. There exists a counterclockwise residual current eddy beneath Topped wall Angle, and it is timed with a clockwise residual current eddy above Topped wall Angle. The river's discharge has little impact on Channel A, but it significantly affects Channels B and C.”*

**Point 14: Do  $T_{xx}$ ,  $T_{xy}$ , and  $T_{yy}$  in Equation (4) correspond to  $T_{ij}$  in Line 140? If so, the corresponding terms should be explained in relation to the variable symbols.**

Response: Thank you for your meticulous review and valuable feedback. Regarding the terms  $T_{xx}$ ,  $T_{xy}$ , and  $T_{yy}$  in Equation (4), I understand your query. These terms do indeed correspond to  $T_{ij}$ , representing viscous friction, turbulent friction, and differential advection, respectively. In the revised manuscript, I have relocated the description of the hydrodynamic model to Section 3, "Study Area and Settings," to provide clearer background information and model configuration.

Although I have removed the specific descriptions of  $T_{xx}$ ,  $T_{xy}$ , and  $T_{yy}$  from Equation (4), I have provided a detailed account of the hydrodynamic model's setup parameters in Section 3. We believe that this modification will aid readers in better understanding our methodology and will focus the paper more closely on our primary research objectives.

The revised sentence now reads as follows:

“..., *An unstructured grid, finite volume, regional ocean model FVCOM (Chen et al., 2003) was used to simulate the hydrodynamic background and hydrological features. It has been widely used for the study of coastal oceanic and estuarine circulation (Jiang and Xia, 2016; Huang et al., 2008; Lai et al., 2018; Chen et al., 2008).*”

Table 5 Parameters of the hydrodynamic model

Parameter	Value
Shoreline	GSHHS
Bathymetry	ETOPO1 and ADCP in-situ
Grid	0.25 km at the boundaries to 25 m near the coastline
Time period	23/4/2023 00:00-30/4/2023 00:00 (Spring neap tide) 28/6/2022 00:00-1/8/2022 00:00 (High water period)
Manning number	28
Eddy viscosity	Smagorinsky formulation data 0.28 m <sup>2</sup> /s
Time step	300 s
Tidal constituents	M2, S2, K1, O1, N2, K2, P1, Q1
Wind/Sea level Pressure	ERA 5
Validation	Basuo Port Station (19°06' N, 108°37' E) ADCP 01, ADCP 02

**Point 15: Line 202, what does this sentence mean? Is there an error in the expression? It is suggested to change "riverway" in Line 220 to "channel" to better match the scope**

## **of the study.**

Response: Regarding the sentence at Line 202, We have revised it to serve as a transition between Section 2.2 and Section 2.3. This modification clarifies the flow of the text and improves the overall narrative of the paper.

As for the term "riverway" at Line 220, I have replaced it with "channel" to align with the terminology that better fits the scope of our study, as you suggested.

The revised sentence now reads as follows:

*“After examining the influence of waves and currents on sediment transport modeling, we now turn our attention to the specific characteristics of sediment properties in the study area. Section 2.3 provides a detailed account of these properties, which are essential for understanding the local sediment dynamics and will be crucial for the model's calibration and validation processes”*

**Point 16: There are errors in the use of symbols in Table 2. The mean grain diameter and median grain diameter have units, which are represented by  $\phi$ , but the sorting coefficient is a unitless value. The same applies to Table 3.**

Response: Thank you for your observation regarding the use of symbols in Table 2 and Table 3. I have taken your feedback into account and have made the necessary corrections. In response to your concern about the symbols in Table 2, I have removed the units for the sorting coefficient, as it is indeed a unitless value. Additionally, you suggested changing "riverway" to "channel" at Line 220 to better match the scope of the study. This change has also been implemented to maintain consistency in terminology and to ensure that it accurately reflects the focus of our research.

**Point 17: Line 241, the range expression for gravel (>2 mm), sand (2~0.063 mm), silt (0.063~0.004 mm) is problematic; the larger value should be placed after the smaller value. The legend of Figure 5 lacks units.**

Response: Thank you for your comment on Line 241 and the legend of Figure 5. In response to your feedback, I have corrected the range expression for gravel ( $>2$  mm), sand ( $0.063\sim 2$  mm), and silt ( $0.004\sim 0.063$  mm) to ensure that the smaller values are placed before the larger ones, following the standard notation for size ranges. Additionally, I have updated the legend of Figure 5 to include the appropriate units, ensuring that all information is clear and accessible to the reader. I believe these amendments address your concerns and improve the precision and readability of the manuscript.

The revised figure now shows as follows:

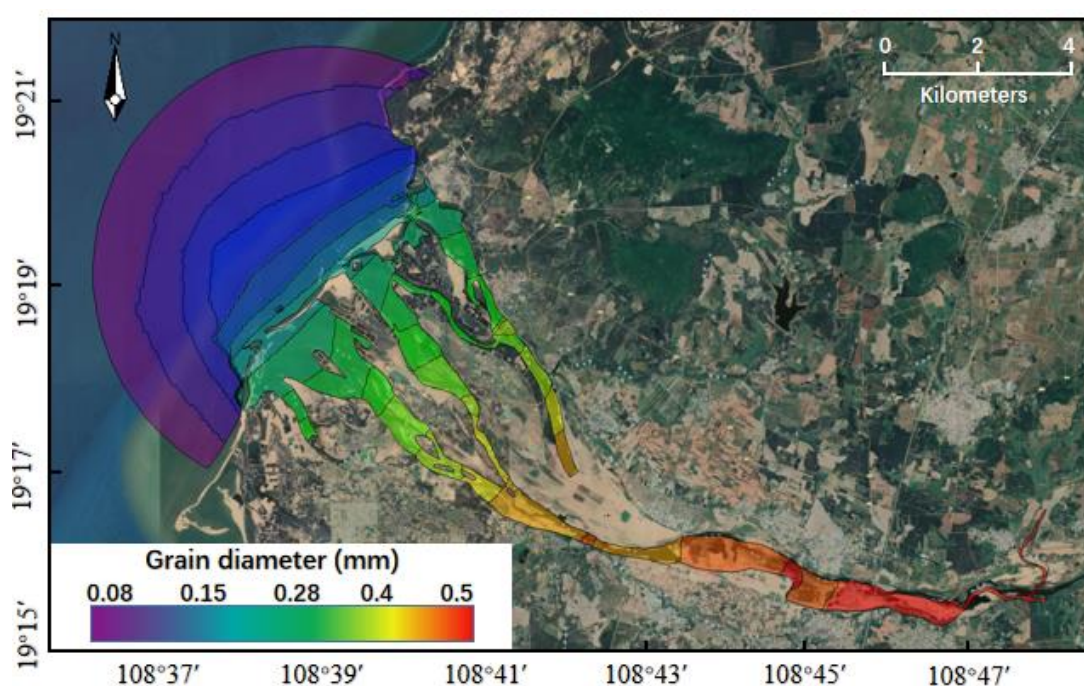


Figure 5 Variation of sediment particle size data (map origination: <https://hainan.tianditu.gov.cn/>)

**Point 18:** The scope of the study in Figure 6 is not consistent with the description in Line 280; it is recommended to modify it. Additionally, according to the geographical location of the Changhua River, it is located in the southwest of Hainan Province, but it is described as the western part in Line 278? Line 287, how is the elevation measured by ADCP obtained? Can specific information about the survey vessel be provided to increase the credibility of the article's data?

Response: Thank you for your continued attention to our manuscript. We have made the

following corrections in response to your comments:

**Figure 6 Scope Consistency:** I have revised the scope depicted in Figure 6 to align with the description provided in Line 280.

**Line 278:** It is important to clarify that while the Changhua River is geographically located in the southwest of Hainan Province, our study focuses on the downstream and estuary areas, which are more accurately described as the western part of Hainan Province when considering the specific segments of the river in question.

**Elevation Measurement by ADCP:** In response to your question about the elevation measurement by ADCP in Line 287, I have included additional details about the survey vessel in the supplementary material. This information provides specific details about the vessel used during the survey, which adds credibility to the data presented in the article.

The revised figure and supplementary material now shows as follows:

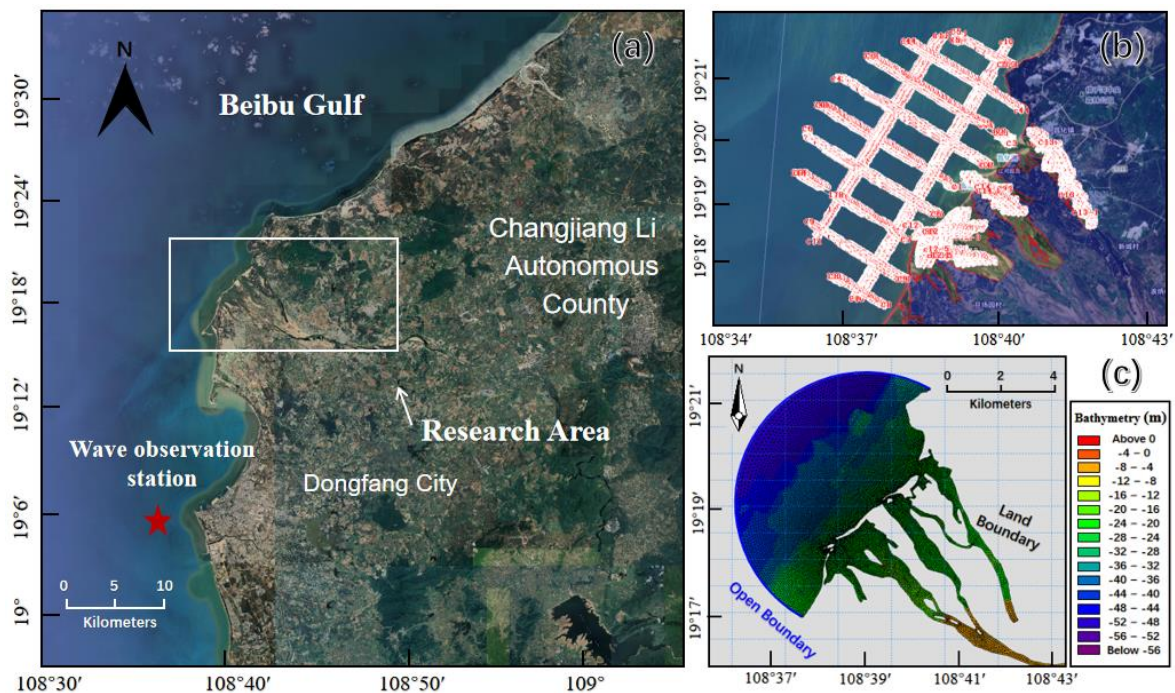


Figure 6 (a) Scope of study area (the white frame) and wave observation (the red star) from Dongfang; (b) ADCP collection points on site; (c) Grids and boundaries (map origination: <https://hainan.tianditu.gov.cn/>)

**Table A.1** List of main parameters of survey vessel

Parameter	Value	Instrument diagram
LOA	11 m	
Breadth	2.8 m	
Modeled Depth	1.2 m	
Design Draft	0.8 m	
Speed	6.0 kn	
Hull Material	Fiber-reinforced plastic (FRP)	

**Point 19: Line 314, remove the comma. "Model validation occurs from 10:00 on April 23, 2023, to 00:00 on April 30, 2023." has an extra comma.**

Response: We sincerely apologize for the typographical error here. We have removed the extra comma as suggested, and the sentence now reads: "Model validation occurs from 10:00 on April 23, 2023 to 00:00 on April 30, 2023."

**Point 20: Section 3.3 lacks analysis of the hydrodynamic results, and the description of the hydrodynamic environment of the study area is insufficient. It is recommended to expand the text and analyze it in conjunction with the sediment transport model.**

Response: Thank you for your feedback on Section 3.3 and the concerns raised about the hydrodynamic results analysis and the description of the hydrodynamic environment in the study area.

We have taken your suggestions into account and have expanded the text in Section 3.3 to include a detailed analysis of the hydrodynamic results. The revised section now discusses the flow field conditions during the flood and ebb tides, as well as during high and low tides, which provides a more comprehensive understanding of the hydrodynamic environment

specific to our study area.

The revised part now reads as follows:

“The hydrodynamic simulation outcomes, as depicted in [Figure 10](#), indicate a predominantly NE-SW reciprocating current pattern within the study area. This flow is aligned parallel to the coastline, with the tidal current shifting direction according to the tidal phase. [Figure 10b](#) and [10c](#) depict the flow field outside the estuary of the Changhua River. [Figure 10b](#) shows the flow field at 23:00 on April 23, 2023, corresponding to the peak of the flood tide. At this time, the tidal current flows in a northeast direction with a maximum speed of 0.62 m/s. [Figure 10c](#) shows the flow field at 13:30 on April 24, 2023, corresponding to the peak of the ebb tide, where the tidal current flows in a southwest direction with a maximum speed of 0.75 m/s. Overall, the tidal currents outside the Changhua River estuary generally follow a northeast-southwest reciprocating pattern, with flood tides flowing northeast and ebb tides flowing southwest, parallel to the shoreline. The maximum ebb current is faster than the maximum flood current.

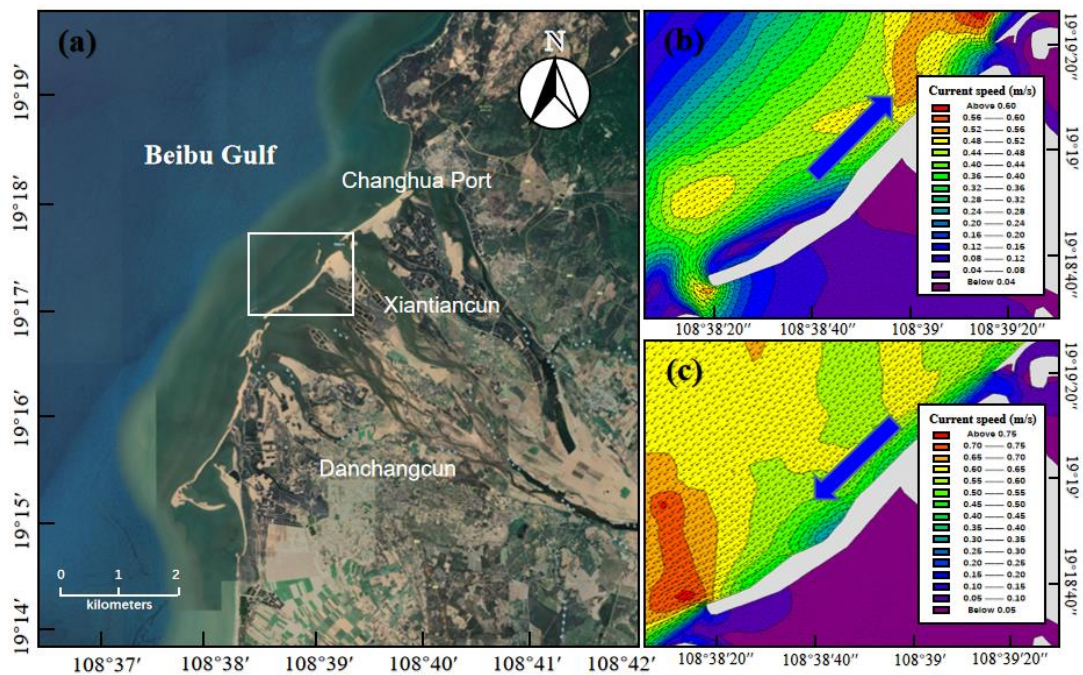


*Figure 10* Study area and coastal current direction: (a) location map of the study area; (b) detailed zoom of the map in [Fig. 9a](#) with NE current; (c) detailed zoom of the map in [Fig. 9a](#) with SW current. (map origination: <https://hainan.tianditu.gov.cn/>)

Figures 11a and 11b illustrate the flow field inside the estuary of the Changhua River. Figure 11a shows the flow field at 23:00 on April 23, 2023, corresponding to the peak of the flood tide. Inside Estuary A, due to the topography, a large counterclockwise circulation forms around the central island, accompanied by several smaller vortices, with the overall trend of tidal currents flowing southeast along the river channel. In Estuary B, ocean inflows meet with river flows from upstream, ultimately converging into Estuary C through the passage between B and C. In Estuary C, the flow is more unidirectional compared to A and B, with upstream water flowing into the ocean, then following the northeast-directed tidal current outside the Changhua River estuary. Figure 11b shows the flow field at 13:30 on April 24, 2023, at the peak of the ebb tide. At this time, the circulation inside Estuary A reverses to a clockwise direction, and other smaller vortices change direction accordingly, with the overall trend of tidal currents flowing from upstream to the ocean. In Estuary B, the dominant force is the high-speed flow from Estuary C, which enters B through the narrow passage between B and C, splitting into two opposite directions: one part flows into the ocean, and the other flows upstream, forming a circulation within the river channel. In Estuary C, the water flows upstream from the ocean along the river channel.

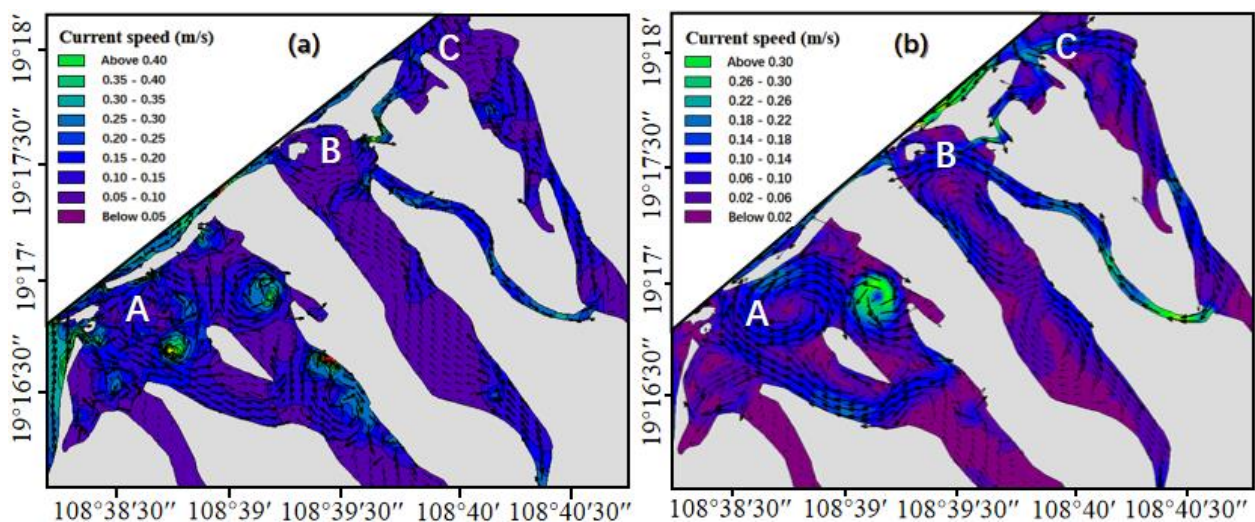


Figure 11 Flow field inside the estuary :(a) moment of the maximum flood current; (b) moment of the maximum ebb current

*To further analyze the characteristics of the flow field in the study area, flow fields are selected for analysis during the transition from low tide to high tide and from high tide to low tide. Figure 12f depicts the location of the research area. Figure 12a shows the flow field at low tide, where the tidal current outside the estuary flows northeast, and water in the main river channel downstream of the Changhua River flows upstream from the ocean. After low tide (during flood tide), water flow velocity gradually increases, with the tidal current outside the estuary consistently flowing northeast. During this period, the main river channel maintains an eastward flow.*

*Figure 12b illustrates the moment of flow direction change during flood tide, when the flow direction outside the estuary rotates clockwise along the shoreline from the south (toward Beili Bay). The northern ocean current (outside Changhua Harbor) also begins to rotate clockwise, flowing into Estuary C, then into the ocean through the passage between B and C, forming a circulation that enhances the clockwise rotation of the northern ocean current. Subsequently, the flow direction gradually changes from northeast to southwest as it moves from the coast toward the open sea. The sand spit at the downstream estuary alters the flow direction and velocity. The sand spit can act as a natural barrier, causing the tidal current to change direction earlier during flood tide.*

*Figure 12c shows the flow field at high tide, where the tidal current outside the estuary has fully shifted to the southwest, while the flow direction further offshore is still transitioning. In the main river channel, the water flows from upstream toward the ocean. Estuaries B and C are influenced by the coastal current outside the northern part of the study area, flowing into the estuary opposite to Estuary A. After high tide (during ebb tide), the water flow velocity in the study area gradually increases, with the tidal current outside the estuary consistently flowing southwest. After some time, the water currents in the southern and northern parts of the study area turn counterclockwise, and the flow direction in the B and C channels changes from inward to outward.*

*Figure 12d shows the flow field at the moment when the flow direction changes during ebb tide. It is evident that there are two counterclockwise circulations outside the Changhua River estuary: one from Beili Bay and the other from outside Changhua Harbor. The latter has a broader influence and thus plays a dominant role in determining the water flow direction in the study area, gradually shifting the coastal current from southwest to northeast. Figure 12e shows the flow field at low tide once again, where the water flow outside the estuary has shifted back to the northeast, repeating the previous flow pattern.*

*In summary, during the transition from flood to ebb tide, the flow field outside the estuary is driven by the deflection of water currents from Beili Bay and Changhua Port, shifting the flow direction from northeast to southwest. During the transition from ebb to flood tide, the deflection is primarily influenced by the circulation outside Changhua Port, shifting the flow direction from southwest to northeast. In channels A, B, and C within the study area, the flow direction changes are relatively consistent due to the passage between B and C. The flow direction in channel A aligns with the main river channel, flowing inward during flood tide and outward toward the ocean during ebb tide.*

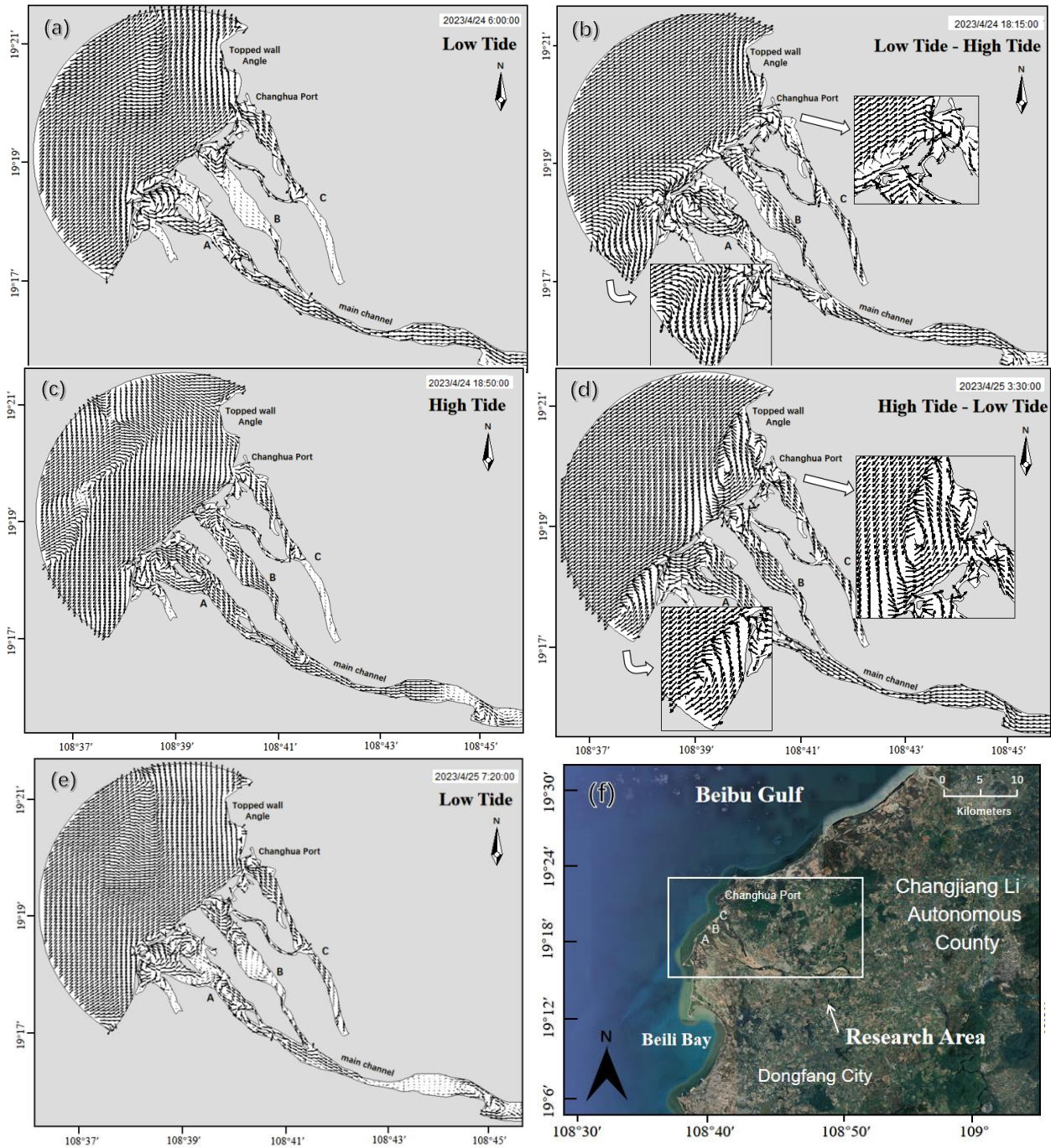


Figure 12 Transition of the flow field (a-e) and location of the study area (f)

”

Point 21: Is the "Code for Design of River Regulation" mentioned in Line 370 some kind of authoritative provision? There are no citations of any literature on this regulation in the text. Is this method applicable to the lower reaches of the Changhua

## River?

Response: Thank you for your comment regarding the "Code for Design of River Regulation" mentioned in Line 370. Upon reflection, we acknowledge the importance of citing authoritative provisions and discussing the applicability of methods to the specific context of our study.

In response to your feedback, we have decided to remove Section 3.4.1, as we have not provided adequate citation or discussion of its applicability to the lower reaches of the Changhua River. We recognize that including such references without proper context or citation could potentially mislead readers.

**Point 22: Line 408, only the first appearance of an abbreviation in the article needs to be spelled out in full; SSC can be expressed directly here.**

Response: Thank you for your guidance on the use of abbreviations in the manuscript. We have revised Line 408 accordingly and now directly use the abbreviation "SSC" for Suspended Sediment Concentration without spelling it out in full, as it was previously defined in the article. This change aligns with the standard practice of abbreviating terms after their initial mention.

The revised part now reads as follows:

*“To further analyze the simulation validation, [Figure 13](#) presents a histogram of the daily absolute error in SSC at Baoqiao Station. The absolute error is calculated as the absolute difference between the measured and simulated values..... The MAE in SSC for Baoqiao Station in July is 0.071224 kg/m<sup>3</sup>. .... Overall, the difference between the daily observed SSC values and the simulated results at Baoqiao Station in July is within a reasonable range, indicating that the model has an acceptable level of precision.”*

**Point 23: The simulation results of the sediment transport model only analyze the thickness changes of the sediment, without a detailed description of the specific movement of the sediment. The measures for sediment control mentioned in Section 4 do not propose a specific implementation plan. It is suggested to revise the content of Section 4, combine the simulation results of the sediment transport model with the hydrodynamic results, and analyze the movement of sediment driven by water flow.**

Response: Thank you for your constructive criticism regarding the sediment transport model analysis in Section 4 of our manuscript. We have taken your suggestions to heart and have thoroughly revised the section to provide a more comprehensive perspective on the sediment movement driven by water flow dynamics. In the updated Section 6, we have expanded our discussion to focus on the critical role of residual currents in sediment transport. Our analysis now includes a detailed examination of the behavior of residual currents during periods of high and low water levels. This comparative analysis offers insights into how these currents influence sediment dynamics under varying environmental conditions, particularly in the context of the lower reaches of the Changhua River.

*Once again, we appreciate the time and effort you and the reviewers have dedicated to evaluating our manuscript. Your expertise and guidance have been invaluable in strengthening our research!*